



PAPER

[View Article Online](#)
[View Journal](#) | [View Issue](#)Cite this: *Dalton Trans.*, 2025, **54**, 8142

A tridentate and dianionic N-heterocyclic olefin (NHO) with two unsymmetrically-tethered aryloxyde sidearms on bismuth: a fortuitous followed by systematic discovery†

Santu Goswami,^a Subham Sarkar,^{a,b} Anisha Guha Roy,^a Dibyendu Mallick ^{*b} and Debabrata Mukherjee ^{*a}

Herein, we report our previously developed bifunctional imidazolium-phenol **LH₂Br** ([HO-4,6-^tBu₂-C₆H₂-2-CH₂{CH(NCH = CHNAr)}]Br; Ar = Dipp = 2,6-ⁱPr₂-C₆H₃), leading to three distinct outcomes with bismuth by simply altering the relative ratios of the reacting components. Treating **LH₂Br** and Bi(HMDS)₃ (HMDS = N(SiMe₃)₂) in a 1:1 ratio gives the NHC-Bi complex [(L)BiBr(HMDS)] (**1**). In contrast, **LH₂Br**, Bi(HMDS)₃, and KHMDS in a 2:1:1 ratio serendipitously result in an unprecedented NHO-Bi complex [(^{Dipp}NHO^{2ArO})BiBr] (**2**), featuring a novel dianionic and tridentate NHO ligand with two unsymmetric aryloxyde sidearms. A tri-acidic imidazolium salt **L'H₃I** ([HO-4,6-^tBu₂-C₆H₂-2-CH₂{C(HO-4,6-^tBu₂-C₆H₂-2-CH₂)(NCH = CHNMe)}]I) is synthesized independently as a potential precursor to such an NHO framework, and the corresponding NHO-Bi complex [(^{Me}NHO^{2ArO})Bi(μ-I)]₂ (**3**) is made as proof of concept. Lastly, treating **LH₂Br** and Bi(HMDS)₃ in a 2:1 ratio also unexpectedly leads to an 'abnormal' NHC-Bi complex [(^{Ar}L)BiBr₂(^{Dipp}Imd)] (**4**; ^{Dipp}Imd = Dipp-imidazole). The multi-component and essentially multi-step reactions leading to **2** and **4** are challenging to fully elucidate mechanistically. Still, control experiments indicate **1** as a possible intermediate in both cases. Based on these results and prior insights into **LH₂Br** and an intermediate **LH**, plausible routes for both **2** and **4** are hypothesized. DFT calculations are also performed to analyze the bonding in **2** and **3** and to justify an NHC to aNHC isomerization towards the formation of **4**.

Received 23rd March 2025,
Accepted 24th March 2025

DOI: 10.1039/d5dt00706b

rsc.li/dalton

Introduction

N-Heterocyclic carbenes (NHCs; Fig. 1) have truly ushered in a new era in chemistry.¹ More importantly, their easy tunability by functionalizing with extra donors has significantly enhanced their scope and versatility as a ligand class.² Alkylidene-appended NHCs, better known as N-heterocyclic olefins (NHOs; Fig. 1), have distinct properties such as high nucleophilicity and strong basicity but nearly no π-acidity.³ Although reported even before the first stable NHC,⁴ NHOs remained mostly dormant for a fairly long time. However, they have gained significant

attention over the past decade, making major contributions in organocatalysis, CO₂ fixation, small molecule activation, polymerization, frustrated Lewis pairs, and, importantly, as neutral 2e⁻ C-donor ligands.⁵ In fact, NHOs have often matched or even outperformed NHCs in various aspects.^{5b} NHO to metal bonds can adapt to varying stereoelectronic demands, which is considered beneficial for catalytic cycles.⁶

Curiously, despite their potential, tailoring NHOs with extra donors has been explored only sporadically, unlike the numerous cases of NHCs.^{5c} A systematic push in this direction is thus essential to further advance NHO chemistry. Iglesias and Oro reported a 'PCP' pincer featuring an NHO with two flexible phosphine arms (Fig. 1).^{6,7} While its cationic Ir complexes **A** and **B** catalyze transfer hydrogenation and solvent-free dehydrogenation of HCO₂H, respectively, the chloride complex **C** isomerizes into its 'abnormal' NHC (aNHC) version at only 40 °C.^{6b,7} The 'OCO' pincer in **D** is non-chelating (Fig. 1) and undergoes a similar NHO to aNHC isomerization at 70 °C.^{6b} This isomerization is an inherent issue as aNHCs are seemingly better donors.⁸ In some cases, even the synthetic conditions and the ligand substituents or metal precursors dictate

^aDepartment of Chemical Sciences, Indian Institute of Science Education and Research Kolkata, Mohanpur, 741246 West Bengal, India.

E-mail: d.mukherjee@iiserkol.ac.in

^bDepartment of Chemistry, Presidency University, 86/1 College Street, Kolkata, 700073 West Bengal, India. E-mail: dibyendu.chem@presiuniv.ac.in† Electronic supplementary information (ESI) available: Spectroscopic data, computational details, and crystallographic data files. CCDC 2348036 (**1**) 2348037 (**2**), 2348038 (**3**), 2348039 (**4**). For ESI and crystallographic data in CIF or other electronic format see DOI: <https://doi.org/10.1039/d5dt00706b>

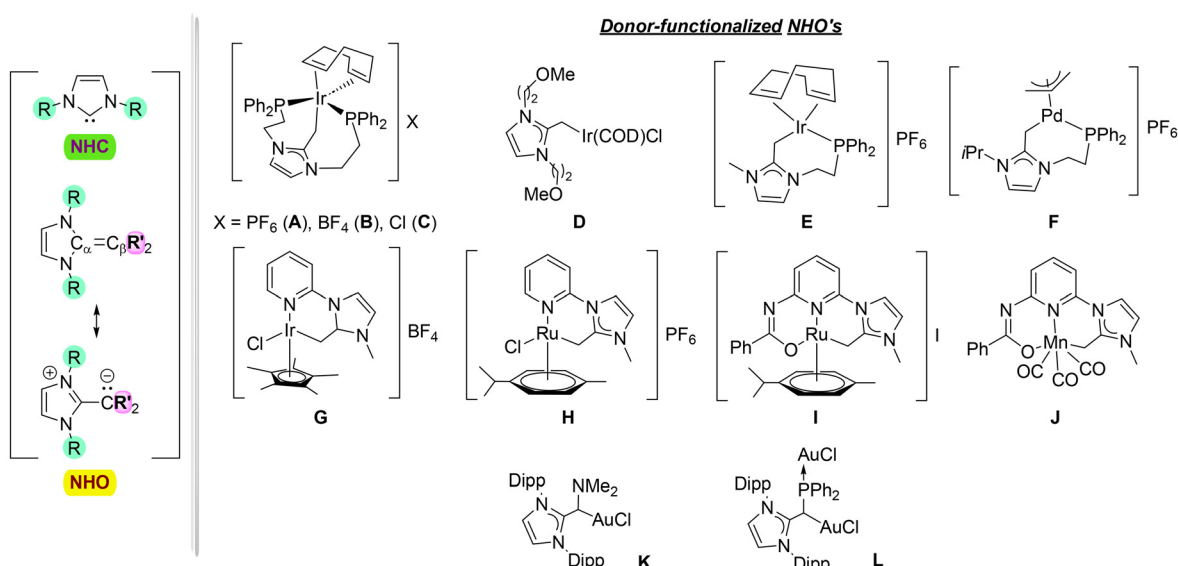


Fig. 1 (left): NHC and NHO frameworks with possible sites for donor functionalization highlighted in green (wingtips) and pink (NHO-C β). (right): selective examples of donor-functionalized NHO complexes previously known.

the choice between NHO and α NHC or can give mixtures of both. Examples (Fig. 1) from Li, Zhao, and Zhang (E, F),⁹ Bernhard and Albrecht (G),¹⁰ and Bera (H)¹¹ with pyridine or phosphine sidearms and metals like Ru, Rh, Ir, and Pd also face the isomerization issue. Bera's pyridyl-based 'ONC' pincer has an NHO on the side (I, J).

The additional donor function(s) in all of these cases are invariably appended to the *N*-wingtip(s) of imidazoline. However, an NHO can also afford an additional donor at its exocyclic C β position. The resulting chelation might be more effective in resisting unwanted isomerization. Rivard made NHOs with an amine or a phosphine donor, but those are

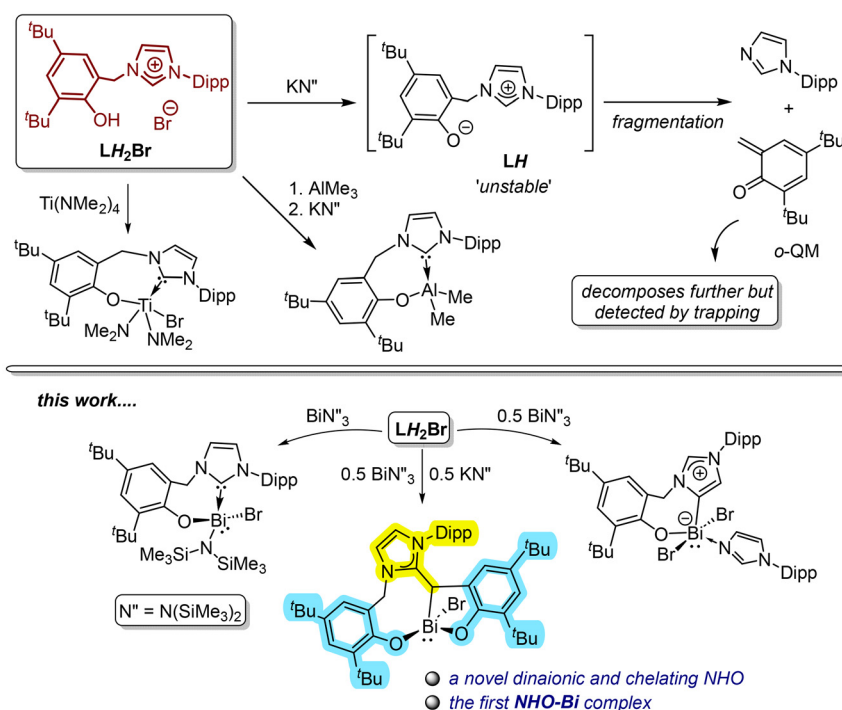


Fig. 2 (top): Bifunctional imidazolium-phenol ligand precursor **LH₂Br**, the corresponding Ti and Al complexes, and the fragmentation of the zwitterionic **LH**; (bottom): a summary of the present work where the same **LH₂Br** is shown to give a NHC-Bi, an α NHC-Bi, and an NHO-Bi complex simply by varying the relative ratios of $\text{Bi}(\text{HMDS})_3$ and KHMDs .

directly bonded to the C β and are non-chelating (**K**, **L**; Fig. 1).¹² The NHO-phosphine binds to two AuCl molecules, one through the phosphorus and the other through the NHO-C β (**L**).^{12b} Besides, Clot and Peris reported a -CH $_2$ -linked NHO-*a*NHC combo and its cationic Ir complex.¹³ A few bis-NHOs are also known, but they are not ligands.¹⁴ A few chiral NHOs are also there.¹⁵

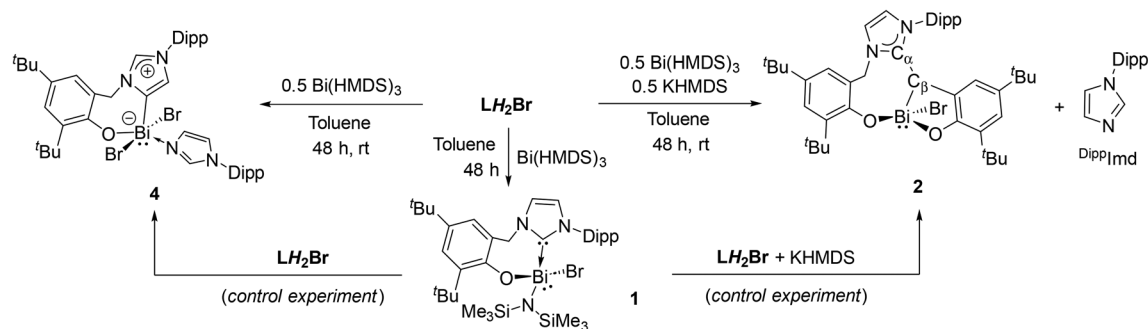
We recently explored a bidentate NHC-aryloxide hybrid ligand [^{Dipp}NHC-CH $_2$ -ArO]⁻ (**L**⁻; Ar = Dipp = 2,6-ⁱPr $_2$ -C $_6$ H $_3$; **LH $_2$ Br** = [HO-4,6-^tBu $_2$ -C $_6$ H $_2$ -2-CH $_2$ {CH(NCH = CHNAr)}]Br), with a flexible -CH $_2$ - linker, on d⁰ metals such as Ti^{IV} and Al^{III} (Fig. 2).¹⁶ **LH $_2$ Br**'s deprotonation by MHMDS (M = Li, K; HMDS = N(SiMe $_3$) $_2$) is also investigated in details,¹⁷ in which the zwitterionic intermediate **LH** undergoes an intriguing fragmentation pattern (Fig. 2).¹⁷ Considering the recent surge in bismuth organometallics¹⁸ but the paucity of its NHC chemistry,¹⁹ we started probing **L**⁻ on Bi^{III} and the present report is on the findings thereof. With Bi, **LH $_2$ Br** interestingly leads to three distinct cases, giving an NHC-Bi^{III}, an NHO-Bi^{III}, and an *a*NHC-Bi^{III} complexes with aryloxide sidearms by simply varying the ratios of Bi(HMDS) $_3$ and KHMDS (Fig. 2). The dianionic and tridentate NHO ligand framework is especially appealing because of its novelty and unsymmetric nature. Both the NHO-Bi and *a*NHC-Bi complexes seem to involve perplexing and essentially multi-step formative routes, which we attempt to postulate based on control experiments and prior insights on **LH $_2$ Br** and the intermediate **LH**. Furthermore, the same NHO framework with a substitutional change is made independently through a systematic design as proof of concept.

Results and discussion

The phenolic O-H (pK $_a$ ~ 12) of **LH $_2$ Br** is more acidic than its imidazolium-2-*H* (pK $_a$ ~ 20) as seen in Al-chemistry.^{16b} **LH $_2$ Br** and Bi(HMDS) $_3$ in a 1 : 1 ratio react slowly over 48 h in toluene to give the NHC-Bi complex [(**L**)BiBr(HMDS)] (**1**; Scheme 1) as a yellow solid. The relatively long reaction time was likely due to the slower deprotonation of imidazolium-2-*H* by moderately basic Bi-HMDS. While monitoring the reaction at the NMR scale, the peaks attributed to complex **1** were visible only from

roughly the 24 h mark. This result also supports the stepwise double deprotonation of **LH $_2$ Br** by Bi(HMDS) $_3$. The Bi center in **1** is 'stereogenic' with four different substituents along with a stereoactive lone pair *trans* to the NHC (Fig. 3). However, without chiral resolution, it exists as a racemic mixture. X-ray diffraction analysis shows the presence of both enantiomers in the asymmetric unit. However, the poor data quality prevented us from further discussing the metric parameters. **1**'s ¹H NMR spectrum in C $_6$ D $_6$ unusually splits the Bi-N(SiMe $_3$) $_2$ signal into two slightly broad singlets (9 H each), most likely due to structural rigidity in the complex that seems to make the two SiMe $_3$ groups distinguishable on the NMR timescale. The linker -CH $_2$ protons are diastereotopic as well.

While studying the coordination of the bulky **L**⁻ on Ti^(IV), trying to fit two **L**⁻ on a single Ti^{IV} center failed and instead led to fragmentation of the ligand framework.^{16a} Since Bi^(III) [*r*_{ionic} (C.N. = 6; C.N. = coordination number): 1.03 Å] is larger than Ti^(IV) [*r*_{ionic} (C.N. = 6): 0.605 Å], we reconceived the idea of placing two **L**⁻ on a single metal, this time on a Bi^(III). As two **LH $_2$ Br** requires four HMDS units to be fully deprotonated, a 2 : 1 : 1 reaction of **LH $_2$ Br**, Bi(HMDS) $_3$, and KHMDS is thus formulated to expect a complex like [(**L**) $_2$ BiBr]. However, surprisingly, the reaction gives an unexpected Bi-complex [(^{Dipp}NHO^{2ArO})BiBr] (**2**; Scheme 1), with a dianionic and tridentate NHO ligand having two distinct aryloxide sidearms. **2** is the only isolable Bi-containing product obtained in a 40% yield as an orange solid. In addition, Dipp-imidazole (^{Dipp}Imd) was identified as a major byproduct in the NMR spectrum analysis of the crude product. The X-ray-determined solid-state structure of **2** (Fig. 4) again shows stereogenic Bi with a four-coordinate distorted trigonal pyramidal geometry, where the stereoactive lone pair is *trans* to the NHO-C β . While one ArO⁻ is tethered to an *N*-wingtip through a -CH $_2$ - linker, the other is directly connected to the NHO-C β . The tridentate and flexible NHO framework leads to rare 8,5-metallacycles upon chelation in *facial* mode. The C β -Bi bond is 2.310(4) Å long. Notably, **2** is the first NHO-Bi complex. The ¹H NMR spectrum of C $_6$ D $_6$ shows the C β -H at 4.14 ppm, which overlaps with one of the two diastereotopic -CH $_2$ - protons. The four inequivalent ^tBu groups gave four individual singlets (9 H each) within 1.40–1.67 ppm. The Dipp-CHMe $_2$ protons gave four doublets



Scheme 1 Bifunctional **LH $_2$ Br** leading to NHC-Bi (**1**), NHO-Bi (**2**), and *a*NHC-Bi (**4**) complexes by reacting with varying ratios of Bi(HMDS) $_3$ and KHMDS.



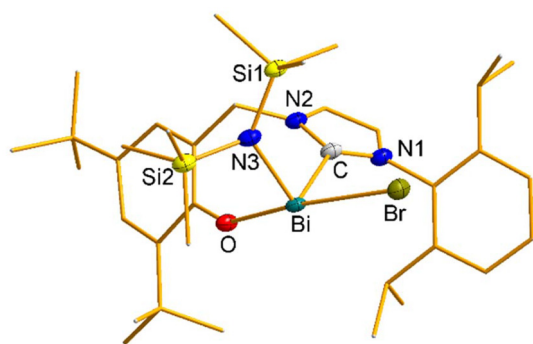


Fig. 3 DIAMOND²⁰-rendered molecular structures of NHC-Bi complex **1**. Relevant ellipsoids are set at a 50% probability level, while the rest of the skeleton is shown as sticks for better viewing. The H atoms and Co-crystallized toluene molecules are omitted for clarity.

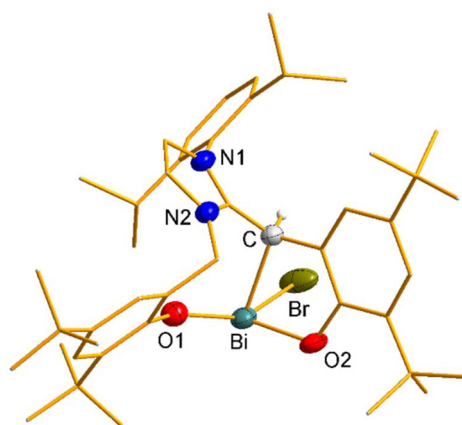


Fig. 4 DIAMOND-rendered molecular structure of the NHO-Bi complex **2**. Relevant ellipsoids are set at a 50% probability level, while the rest of the skeleton is shown as sticks for better viewing. All H atoms except the NHO-C_{ip}H are omitted for clarity. Selected bond distances (Å): Bi–C 2.310(4), Bi–O1 2.236(3), Bi–O2 2.115(3), Bi–Br 2.8244(7). Selected bond angles (°): ∠C–Bi–O2 79.7(1), ∠C–Bi–Br 82.7(1), ∠C–Bi–O1 87.2(1), ∠O2–Bi–Br 97.3(1), ∠O1–Bi–Br 151.4(1), ∠O1–Bi–O2 107.1(1).

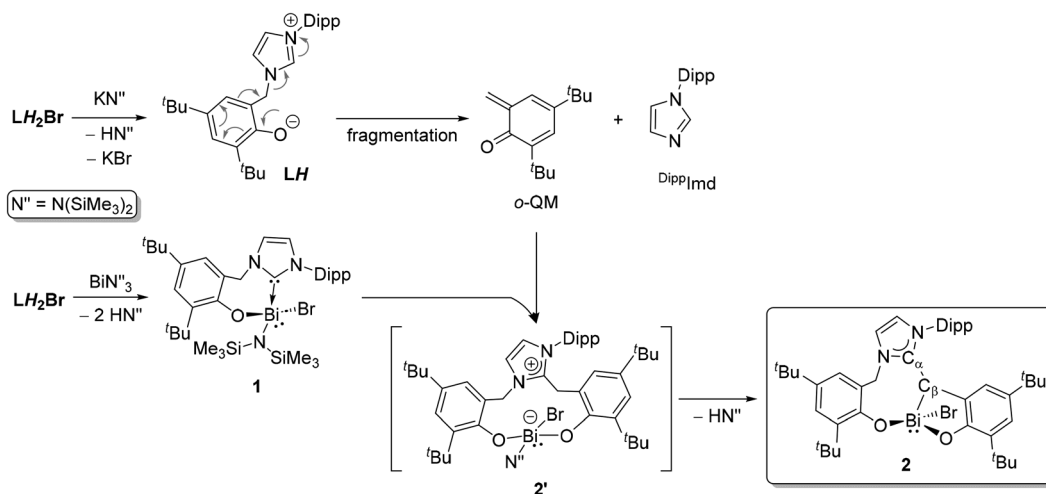
within 0.87–1.39 ppm and the two methine protons as two septets at 2.53 and 2.82 ppm, respectively. The olefinic backbone of NHO gives two overlapping peaks at 5.75 ppm (2 H).

The composition of **2** suggests a complex route of formation, seemingly with partial ligand fragmentation and a C–C bond formation. Monitoring the reaction at the NMR scale revealed a perplexed spectral pattern with broad and overlapping resonances. The reaction mixture is also partly inhomogeneous throughout because the starting **LH₂Br** and byproduct KBr are insoluble in toluene (Fig. S7; ESI[†]). Resonances attributed to **2** are noted at approximately the 24 hour mark and continue to grow over the next 24 h. However, the overall spectral pattern is complex and difficult to interpret. Thus, mechanistically elucidating this multi-component and visibly multi-step reaction is challenging. As shown in Fig. 2, our previous knowledge suggests that **LH₂Br** undergoes rapid deprotonation by KHMDS to give **LH** that is

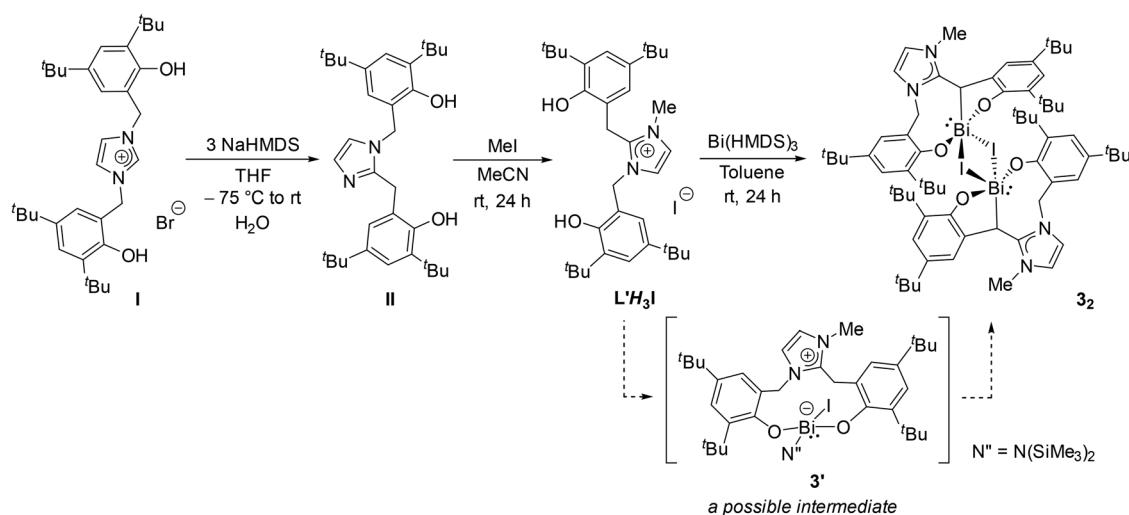
unstable and fragmented into ^{Dipp}Imd and an *o*-quinone methide (*o*-QM).¹⁷ The latter is more fleeting and was only detected by trapping with maleic anhydride.¹⁷ The timeline for the formation of **2** (48 h) is roughly similar to that of the **LH** fragmentation. In a control experiment, reacting **1** with freshly generated **LH** also gives **2** within a similar time and in a similar yield of 40%. Therefore, **1** could be an intermediate towards the formation of **2**. In another experiment, the addition of **1** was performed after incubating the *in situ* generated **LH** for 24 h, which decreased the yield of **2** to only 10%. This suggests that the *o*-QM is the coupling partner of **1** for constructing the NHO framework. The induction period allows the *o*-QM to degrade profoundly before it can couple with **1**, which can explain the drop in **2**'s yield. Based on these limited insights, a plausible pathway (Scheme 2) was theorized for the formation of **2** involving two parallel 1 : 1 reactions of **LH₂Br**, one with KHMDS and the other with Bi(HMDS)₃. While KHMDS would produce **LH** and subsequently the *o*-QM and ^{Dipp}Imd, Bi(HMDS)₃ and the 2nd **LH₂Br** would give **1**. Given the relatively weaker nature of an NHC–Bi bond,^{19a,b} the NHC in **1** is presumed to capture the *o*-QM as the C–C bond-forming step to give a zwitterionic complex **2'**. Intramolecular deprotonation from **2'** by the remaining HMDS on Bi can then possibly yield **2**. Notably, replacing KHMDS with other bases such as LiHMDS or KO^tBu, while keeping the other reaction parameters the same gives only complex mixtures with no sign of **2**. Crystallization attempts have also not afforded any identifiable species so far. This suggests the formation of **2** from **LH₂Br** as base-specific, which is not surprising given the already observed dichotomic behavior of **LH₂Br** towards two equiv. of KHMDS and LiHMDS.¹⁷

Given the complex formation of **2** with a dubious mechanistic understanding, we aimed to devise an independent and more controlled synthetic route for this novel NHO framework with options for substitutional variation. Thus, NHO can also be applied to other metals. This is achieved by starting from the bis-phenolic imidazolium salt **I** (Scheme 3).²¹ A triple deprotonation of **I** by NaHMDS followed by an aqueous workup gives the bis-phenolic imidazole **II**.²¹ The reaction proceeds *via* an NHC intermediate followed by its 1,2-benzyl migration.²¹ Treating **II** with MeI gives a new imidazolium salt **L'H₃I** [(HO-4,6-^tBu₂-C₆H₂-2-CH₂{C(HO-4,6-^tBu₂-C₆H₂-2-CH₂)(NCH = CHNMe)}]I, a potential tri-acidic precursor for such an NHO framework. Reacting **L'H₃I** and Bi(HMDS)₃ in a 1 : 1 ratio under the same conditions as used for obtaining **1** and **2** indeed gives the NHO-BiI [(^{Me}NHO^{2ArO})Bi(μ-I)]₂ (**3₂**; 76%) as another orange solid. Given the relatively higher acidity of the phenols than the –CH₂– linker in **L'H₃I**, we believe the three-fold deprotonation of **L'H₃I** to give **3** is not concerted and should go through an intermediate like **3'** (Scheme 3). The similarity between **3'** and **2'** indirectly supports the route for **2** *via* **2'** proposed in Scheme 2. Solid **3₂** is a centrosymmetric dimer (Fig. 5), as confirmed by X-ray analysis. The dimeric nature of **3₂**, unlike that of the monomeric **2** is likely due to the smaller *Me* than *Dipp* as the *N*-substituent on the NHO imidazole unit and the higher bridging aptitude of iodide





Scheme 2 A plausible mechanistic route towards the formation of the NHO-Bi complex **2**.



Scheme 3 Independent synthesis of an NHO ligand precursor related to the one in **2** and its Bi complexation.

than bromide. However, the DOSY analysis of THF- d_8 indicated that monomeric **3** was present in solution (see ESI†). The C_β -Bi bond is 2.298(5) Å long, similar to that in **2**. The other relevant metric parameters are also in the same range.

The bonding in **2** and **3₂** were probed using the NBO method at the M06-2X/def2-TZVPP level of theory on structures optimized in the gas phase at the M06-2X/6-31G** (def2-TZVPP for Bi) level (see ESI†). The exocyclic $\text{C}_\beta=\text{C}_\beta$ of the dianionic NHO has Wiberg Bond Indices (WBI) of 1.663 (for *N-Dipp*) and 1.590 (for *N-Me*) because the π -bond is formed by the side-on overlap of the two $2p_{\text{C}}$ orbitals.²² The olefinic nature decreases as the same $2p$ orbital of C_β forms an σ -bond with the vacant $6p$ of Bi (Fig. 6) as indicated by the WBIs of 1.093 and 1.078, respectively in **2** and **3₂**.²² The C_α - C_β is also more polarized in **2** and **3₂** as the C_β is more negatively charged [−0.688 (**2**; Fig. 6), −0.711 (**3₂**)] than in their non-metalated

NHOs (−0.373 (*N-Dipp*); −0.421 (*N-Me*)). Thus, the NHO-Bi interaction increased the ylide character as expected.

Considering the 2 : 1 : 1 stoichiometry of **LH₂Br**, KHMDs, and Bi(HMDS)₃ in the formation of **2**, two more control experiments are conducted by reacting **LH₂Br** individually with KHMDs and Bi(HMDS)₃ in 2 : 1 ratios. The KHMDs case results the same as in the 1 : 1 reaction,¹⁷ giving **LH** and ultimately its fragmentation, while the 2nd equiv. of **LH₂Br** remains untouched. However, Bi(HMDS)₃ leads to another unexpected Bi-complex [(^aL)BiBr₂(^{Dipp}Imd)] (**4** (77%); Scheme 1) as one more orange solid, this time with an aryloxy-tethered ‘abnormal’ NHC. The monomeric form and mesoionic nature of the carbene are established by X-ray diffraction analysis (Fig. 7). The Bi in **4** has a distorted square-pyramidal geometry with its stereoactive lone pair *trans* to the *a*NHC. Despite the higher coordination number of the Bi



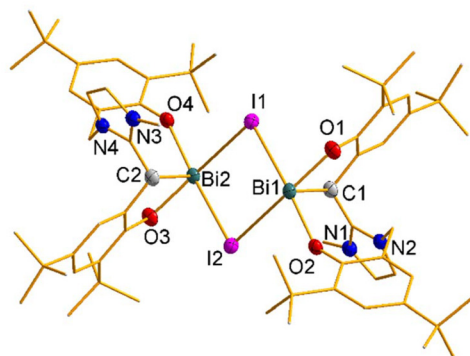


Fig. 5 DIAMOND-rendered molecular structure of **3₂**. Relevant ellipsoids are set at a 50% probability level, while the rest of the skeletons are shown as sticks for better viewing. The H atoms and co-crystallized THF molecules are omitted for clarity. Selected bond distances (Å): Bi1–C1 = Bi2–C2 2.298(5), Bi1–O1 = Bi2–O3 2.158(4), Bi1–O2 = Bi2–O4 2.227(3), Bi1–I1 = Bi2–I2 3.1972(4), Bi1–I2 = Bi2–I1 3.3270(4). Selected bond angles (°): [**3₂**]: ∠C2–Bi2–O4 = ∠C1–Bi1–O2 79.7(1), 79.7(1), ∠C2–Bi2–O3 = ∠C1–Bi1–O1 78.7(1), 78.7(1), ∠Bi1–I1–Bi2 = ∠Bi1–I2–Bi2 97.1(1), ∠C1–Bi1–I1 = ∠C2–Bi2–I2 79.5(1), 79.5(1), ∠C1–Bi1–I2 = ∠C2–Bi2–I1 86.0(1), 79.5(1).

center in **4**, the *a*NHC–Bi bond length (2.248(4) Å) is in the same range as the NHC–Bi in **1** and the NHO–Bi in **2** and **3₂**. This is likely due to the *a*NHC's stronger ligating ability and lower steric bulk.²³

As in the case of **2**, the fortuitous formation and composition of **4** also indicate a complex and multi-step synthetic route with ligand fragmentation. Monitoring it at the NMR scale again showed a complex spectral pattern, which denied the identification of any potential intermediate. Nonetheless, a control experiment by reacting **LH₂Br** and **1** in a 1 : 1 ratio also gives **4** to imply that the latter can also be accessed by starting from **1**, as seen in the case of **2**. Based on this and prior fragmentation insights, a tentative route towards **4** is postulated in Scheme 4. We theorize that the phenolic –OH moieties of two **LH₂Br** can be deprotonated first by Bi(HMDS)₃ to give a zwitterionic species like [**1HBr**] and an equiv. of **LH**. Reacting **1** with an equiv. of **LH₂Br** can also give the same

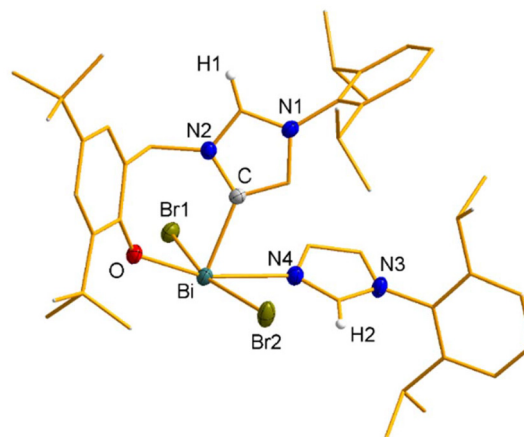


Fig. 7 DIAMOND-rendered molecular structure of the *a*NHC–Bi complex **4**. Relevant ellipsoids are set at a 50% probability level, while the rest of the skeletons are shown as sticks for better viewing. A co-crystallized toluene molecule is omitted for clarity. Only relevant H atoms are shown. Selected bond distances (Å): Bi–C 2.248(4), Bi–O 2.198(3), Bi–N4 2.608(4), Bi–Br1 2.9253(5), Bi–Br2 2.7814(5). Selected bond angles (°): [**4**]: ∠C–Bi–O = 88.0(1), ∠C–Bi–N4 = 76.0(1), ∠C–Bi–Br1 = 87.5(1), ∠C–Bi–Br2 = 85.9(1), ∠O–Bi–N4 = 164.0(1), ∠O–Bi–Br1 = 98.6(9), ∠O–Bi–Br2 = 96.8(8), ∠Br1–Bi–Br2 = 163.0(2), ∠Br1–Bi–N4 = 82.4(8), ∠Br2–Bi–N4 = 80.7(8).

mixture by protonating the NHC of **1**, preferably over its Bi–HMDS. Intramolecular deprotonation from [**1HBr**] can then give a new NHC complex like [(**L**)BiBr₂] (**4'**), whereas the **LH** can be fragmented on the side to furnish ^{Dipp}Imd. The latter can then coordinate to the Bi of **4'** and drive NHC to *a*NHC isomerization to yield **4**. The protonation of a metal-bound NHC in the presence of other potentially basic groups is known with the main group and early transition metal complexes, in which the NHC–metal bonds are inherently weak. For instance, Al-bound NHC can be selectively protonated by ⁱPrOH over the Al–Me.²⁴ Another Al-bound NHC gets selectively protonated by PhOH over Al–ⁱBu.²⁵ In our titanium case, the NHC–Ti bond is selectively protonated by an acidic imidazolium-2-*H* over two Ti-bound NMe₂ moieties.^{16a} The weak

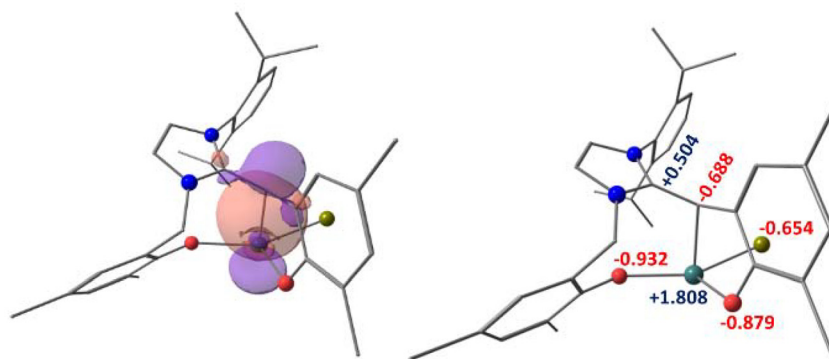
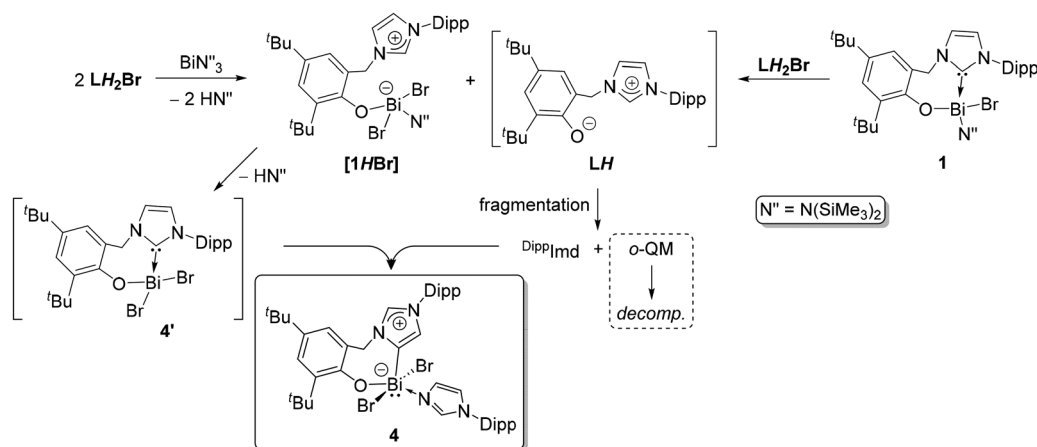


Fig. 6 (left): NBO plot (isovalue = 0.030) showing the NHO–Bi bond in **2**; (right): natural charges on the selected atoms of **2** calculated at the M062X/B2//M062X/B1 level of theory (see ESI†).





Scheme 4 A plausible mechanistic route towards the formation of the aNHC-Bi complex **4**.

nature of an NHC-Bi bond is already noted in the spontaneous isomerization of a (NHC)-BiPhCl₂ complex into its aNHC variant.^{19b}

To further check the viability of this carbene isomerization, the postulated NHC-Bi complex **4'** and its hypothetical aNHC version are first compared by computing the free-energy change involved in replacing the NHC with its abnormal variant (Scheme 5). The same is repeated by considering ^{Dipp}Imd as a coligand (Scheme 5). Calculations suggest that both reactions are exergonic, but their extent is greater in the presence of ^{Dipp}Imd. This observation prompts us to probe the effect of ^{Dipp}Imd on the difference in the Bond Dissociation Energies (BDEs) between the aNHC-Bi and NHC-Bi in concerned complexes (page S14; ESI†).

Here, NHC provides more effective sterics than aNHC on Bi. From the electronic energy calculations (page S14; ESI†), without the ^{Dipp}Imd, **4'** is 3.0 kcal mol⁻¹ lower than [(^aL)BiBr₂]. However, with ^{Dipp}Imd, the order is reversed, as the aNHC-Bi complex (**4**) is 3.0 kcal mol⁻¹ lower than its NHC variant [(L)BiBr₂(^{Dipp}Imd)]. Considering only the ligands, the electronic energy of L⁻ is 12.1 kcal mol⁻¹ lower than that of ^aL⁻. This leads to the bond dissociation energy (BDE) gaps between Bi-C_{aNHC} and Bi-C_{NHC} with and without ^{Dipp}Imd as 15.1 and 9.1 kcal mol⁻¹, respectively (eqn (v), page S15; ESI†).²⁶ This means, in terms of strength, aNHC-Bi is stronger than NHC-Bi for both cases. However, the difference was greater when bulky ^{Dipp}Imd was present on Bi. It essentially weakens the NHC-Bi

bond, as shown by its ~0.05 Å elongation. In contrast, the aNHC-Bi remained virtually unchanged in the presence of ^{Dipp}Imd. Overall, the coordination of ^{Dipp}Imd steers the isomerization. The steric-driven isomerization of NHC to aNHC is known.²⁷ [(IPr)BiBr₃]^{19a} and [(IPr)BiPhCl₂]^{19b} (IPr = 1,3-bis(2,6-diisopropylphenyl)-imidazol-2-ylidene) also exhibited the same properties under different conditions. Notably, mesoionic aNHCs are yet another significant and fast-evolving neutral C-based ligand class, but their donor-functionalized variants are rare, as in the case of NHOs.²³ **4** is the first such example using bismuth.

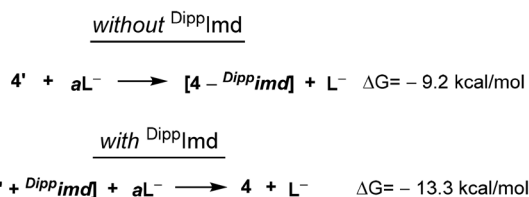
Conclusions

In summary, we made multi-layered discoveries while testing a hybrid NHC-aryloxide ligand framework on bismuth. It leads to the first ever chelating NHC-, NHO-, and aNHC-Bi complexes with aryloxide sidearms, all from the same imidazolium-phenol precursor and by just varying the relative ratios of Bi(HMDS)₃ and KHMDS. The product compositions suggest that the NHC-Bi chemistry, which has been rarely explored, could be mechanistically complex. Nonetheless, an independent synthetic protocol for the precursor to the novel NHO skeleton with substitutional variation should pave the way for exploring other metals in this ligand class. Chelating variants of both NHOs and aNHCs are considerably rarer than those of NHCs. The findings of this study should improve the coordination chemistry of such ligand classes. We are also developing other donor-tethered NHOs and aNHCs.

Experimental

General considerations

All experiments were performed under dry and oxygen-free nitrogen conditions using standard Schlenk techniques or in an argon-filled glovebox (MBraun), unless otherwise stated.



Scheme 5 Hypothetical ligand replacement reactions and the related free-energy changes.



Before use, glassware was dried overnight at 130 °C, and solvents were dried, distilled and degassed using standard methods and stored over activated 4 Å molecule sieves in the glove box. **LH₂Br**, ^{16a} Bi(N(SiMe₃)₂)₃, ²⁸ **I** ²⁹ and **II** ²⁹ were made by following the literature procedure. BiCl₃ and KN(SiMe₃)₂ were purchased from Sigma-Aldrich and used inside the glove-box as received. ¹H and ¹³C{¹H} NMR spectra were recorded on a Bruker Avance NEO (500 MHz) or Avance III (500 MHz) or Jeol (400 MHz) spectrometer at ambient temperature unless otherwise mentioned. Abbreviations for NMR spectra: s (singlet), d (doublet), t (triplet), q (quartet), sept (septet), br (broad). Mass spectrometric analyses were performed on a Bruker micrOTOF-Q II or Waters Xevo G2-XS QToF Spectrometers. Elemental analyses were performed on a PerkinElmer series II 2400 machine. X-ray diffraction data were collected on a Rigaku Synergy i xtalab diffractometer. The crystallographic data for the structures reported in this article have been deposited at the Cambridge Crystallographic Data Centre, under the deposition numbers CCDC 2348036 (**1**) 2348037 (**2**), 2348038 (**3**₂), 2348039 (**4**).†

[(L)BiBr(HMDS)] (**1**)

A 10 mL screw-cap vial fitted with a stir bar was charged with **LH₂Br** (0.528 g, 1.000 mmol) and suspended in 2 mL of toluene. A 3 mL toluene solution of Bi(N(SiMe₃)₂)₃ (0.690 g, 1 mmol) was added dropwise. The reaction mixture was then stirred at room temperature for 48 h to obtain a yellowish-orange homogeneous solution. The volatiles were then removed under reduced pressure to obtain a yellow solid. Washing the solid with hexane (3 × 5 mL) and drying under vacuum gave **1** (0.750 g, 0.838 mmol, 84%) as an analytically pure yellow solid. X-ray quality single crystals were grown from its concentrated toluene solution at −30 °C.

¹H NMR (C₆D₆, 500 MHz): δ 7.59 (s, 1 H, ArH), 7.21 (t, ³J_{HH} = 8.0 Hz, 1 H, ArH), 7.10 (d, ³J_{HH} = 7.5 Hz, 1 H, ArH), 7.01 (m, 2 H, ArH), 6.84 (d, ²J_{HH} = 13 Hz, 1 H, ArCH₂N), 6.34 (s, 1 H, NCHCHN), 6.29 (s, 1 H, NCHCHN), 4.13 (d, ²J_{HH} = 13 Hz, 1 H, ArCH₂N), 2.44 (br, m, 2 H, CHMe₂), 1.69 (s, 9 H, CMe₃), 1.55 (d, ³J_{HH} = 6.5 Hz, 3 H, CHMe₂), 1.39 (s, 9 H, CMe₃), 1.29 (d, ³J_{HH} = 6.5 Hz, 3 H, CHMe₂), 0.97 (d, ³J_{HH} = 6.5 Hz, 3 H, CHMe₂), 0.54 (d, ³J_{HH} = 6.5 Hz, 3 H, CHMe₂), 0.49 (s, 9 H, NSiMe₃), 0.30 (s, 9 H, NSiMe₃). ¹³C{¹H} NMR (C₆D₆, 126 MHz): 162.2 (NCN), 146.6 (Cⁱpr, Dipp), 144.6 (Cⁱpr, Dipp), 139.6 (CN, Dipp), 135.8 (Ar-C, Dipp), 133.6 (Ar-C, Dipp), 131.5 (Ar-C, Dipp), 128.8 (Ph-C), 126.3 (Ph-C), 125.6 (Ph-C), 125.3 (Ph-C), 124.5 (Ph-C), 123.7 (Ph-C), 122.8 (NCHCHN), 122.6 (NCHCHN), 54.5 (PhCH₂N), 35.9 (CMe₃), 34.4 (CMe₃), 32.5 (CHMe₂), 30.9 (CHMe₂), 29.1 (CMe₃), 26.7 (CMe₃), 23.7 (CHMe₂), 23.0 (CHMe₂), 7.8 (NSiMe₃), 4.4 (NSiMe₃). Elemental analysis of C₃₆H₅₉BrN₃OSi₂Bi: Calcd C, 48.32; H, 6.65; N, 4.70; Found C, 48.07; H, 6.73; N, 4.59.

[(DippNHO^{2ArO})BiBr] (**2**)

A 10 mL screw-cap vial fitted with a stir bar was charged with **LH₂Br** (0.528 g, 1.000 mmol) and suspended in 2 mL of toluene. A 3 mL toluene solution of Bi(N(SiMe₃)₂)₃ (0.345 g,

0.500 mmol) and a 2 mL toluene solution of KHMDS (0.100 g, 0.500 mmol) were added into the reaction vial nearly at the same time. The reaction mixture was then stirred for 48 h at room temperature to obtain an orange solution along with some insoluble residues. The filtrate was then filtered through a pad of Celite and evaporated to dryness under reduced pressure to obtain an orange residue. Washing the residue with hexane (3 × 5 mL) and drying under vacuum afforded **2** (0.190 g, 0.200 mmol, 40%) as an analytically pure orange solid. X-ray quality single crystals were grown from a concentrated solution in a toluene/THF solvent mixture at −30 °C.

¹H NMR (C₆D₆, 500 MHz, ppm): δ 7.55 (br, 1 H, ArH), 7.46 (s, 1 H, ArH) 7.12 (s, 1 H, ArH) 7.05 (s, 1 H, ArH) 6.92 (d, ³J_{HH} = 7.5 Hz, 1 H, ArH) 6.81 (s, 1 H, ArH) 6.64 (s, 1 H, ArH), 5.75 (br, 2 H, NCHCHN), 5.49 (d, ²J_{HH} = 14 Hz, 1 H, ArCH₂N), 4.14 (s, 1 H, ArCHBi), 4.11 (d, ²J_{HH} = 14 Hz, 1 H, ArCH₂N), 2.82 (m, 1 H, CHMe₂), 2.53 (m, 1 H, CHMe₂), 1.67 (s, 9 H, CMe₃), 1.53 (s, 9 H, CMe₃), 1.41 (s, 9 H, CMe₃), 1.40 (s, 9 H, CMe₃), 1.39 (d, ³J_{HH} = 6.5 Hz, 6 H, CHMe₂), 1.14 (d, ³J_{HH} = 6.5 Hz, 6 H, CHMe₂), 0.90 (d, ³J_{HH} = 6.5 Hz, 6 H, CHMe₂), 0.88 (d, ³J_{HH} = 6.5 Hz, 6 H, CHMe₂). ¹³C{¹H} NMR (126 MHz, CDCl₃): δ 161.4 (NCN), 147.6 (Cⁱpr, Dipp), 145.6 (Cⁱpr, Dipp), 140.4 (CN, Dipp), 137.8 (Ar-C, Dipp), 132.3 (Ar-C, Dipp), 130.1 (Ar-C, Dipp), 128.6 (Ph-C), 125.3 (Ph-C), 124.6 (Ph-C), 124.2 (Ph-C), 123.6 (Ph-C), 121.4 (NCHCHN), 120.9 (NCHCHN), 35.7 (CCHBi), 35.2 (ArCH₂N), 34.5 (CMe₃), 34.4 (CMe₃), 32.6 (CMe₃), 32.5 (CMe₃), 31.0 (CHMe₂), 30.5 (CHMe₂), 29.2 (CMe₃), 28.3 (CMe₃), 27.5 (CMe₃), 26.3 (CMe₃), 25.9 (CHMe₂), 25.8 (CHMe₂), 24.0 (CHMe₂), 23.0 (CHMe₂). Elemental analysis of C₄₅H₆₂BrN₂O₂Bi: calculated C, 56.78; H, 6.57; N, 2.94; found C, 56.29; H, 6.48; N, 2.98.

II

A 100 mL Schlenk flask fitted with a stir bar was charged with **I** (0.920 g, 1.570 mmol) and suspended in 10 mL of THF. It was then cooled to −78 °C before dropwise adding a 10 mL THF solution of KN(SiMe₃)₂ (0.940 g, 4.710 mmol) *via* a cannula. The reaction mixture was then allowed to come to room temperature slowly before being quenched with an excess of water. Et₂O was then added, and the organic layer was separated. The aqueous layer was further washed with fresh Et₂O (2 × 50 mL), and the combined organic portion was dried with MgSO₄. Removing the volatiles under reduced pressure afforded **II** (0.450 g, 0.891 mmol, 56% yield) as a white solid.

¹H NMR (CDCl₃, 400 MHz): δ 7.28 (s, 1 H, ArH), 7.19 (d, ³J_{HH} = 2.4 Hz, 1 H, ArH), 7.01 (d, ³J_{HH} = 2.4 Hz, 1 H, ArH), 6.74 (b, 1 H, ArH), 6.73 (d, ³J_{HH} = 2.4 Hz, 1 H, NCHCHN), 6.13 (d, ³J_{HH} = 2.4 Hz, 1 H, NCHCHN), 5.14 (s, 2 H, ArCH₂N), 3.92 (s, 2 H, ArCH₂C), 1.44 (s, 9 H, CMe₃), 1.43 (s, 9 H, CMe₃) 1.20 (s, 9 H, CMe₃), 1.06 (s, 9 H, CMe₃). ¹³C{¹H} NMR (CDCl₃, 100 MHz): 153.4 (NCN), 148.9 (Ar-C), 148.3 (Ar-C), 144.1 (Ar-C), 141.3 (Ar-C), 139.7 (Ar-C), 138.4 (Ar-C), 125.9 (Ar-C), 124.6 (Ar-C), 124.3 (Ar-C), 123.7 (Ar-C), 123.3 (Ar-C), 121.9 (NCHCHN), 120.0 (NCHCHN), 47.6 (CCH₂Ar), 35.2 (ArCH₂N), 35.1 (CMe₃), 34.2 (CMe₃), 34.1 (CMe₃), 31.7 (CMe₃), 31.3 (CMe₃), 30.5 (CMe₃), 29.9 (CMe₃). HRMS (M/Z): calculated [M + H] = 505.3800; found 505.3804.



L'H₃I

A Teflon-stopped storage tube fitted with a magnetic stir bar was charged with **II** (0.400 g, 0.792 mmol) and dissolved in 10 mL of acetonitrile. 800 μ L of iodomethane (0.226 g, 1.580 mmol) was added to this solution. The reaction mixture was then placed in an oil bath pre-heated to 90 °C and stirred for 2 h, during which a colourless solid precipitated. The reaction tube was then cooled to room temperature. The solid was then filtered and washed with Et₂O (3 \times 10 mL) and toluene (3 \times 10 mL) successively to obtain **L'H₃I** (0.480 g, 0.742 mmol, 94%) as a white powder.

¹H NMR (DMSO-D₆, 400 MHz): δ 8.47 (s, 1 H, ArOH), 8.25 (s, 1 H, ArOH), 7.71 (d, ³J_{HH} = 2.4 Hz, 1 H, ArH), 7.55 (d, ³J_{HH} = 2.4 Hz, 1 H, ArH), 7.18 (d, ³J_{HH} = 2.4 Hz, 1 H, ArH), 7.13 (d, ³J_{HH} = 2.4 Hz, 1 H, ArH), 6.85 (d, ³J_{HH} = 2.4 Hz, 1 H, NCHCHN), 6.18 (d, ³J_{HH} = 2.4 Hz, 1 H, NCHCHN), 5.37 (s, 2 H, ArCH₂N), 4.51 (s, 2 H, ArCH₂C), 3.62 (s, 3 H, NCH₃), 1.36 (s, 9 H, CMe₃), 1.32 (s, 9 H, CMe₃), 1.11 (s, 9 H, CMe₃), 1.06 (s, 9 H, CMe₃). ¹³C NMR (DMSO-D₆, 126 MHz): 151.5 (NCN), 150.6 (Ar-C), 145.4 (Ar-C), 142.5 (Ar-C), 142.4 (Ar-C), 138.7 (Ar-C), 124.4 (Ar-C), 124.1 (Ar-C), 123.1 (Ar-C), 122.6 (Ar-C), 122.5 (Ar-C), 122.4 (NCHCHN), 121.7 (NCHCHN), 47.7 (CCH₂Ar), 35.0 (ArCH₂N), 34.7 (N-Me), 33.9 (CMe₃), 33.7 (CMe₃), 31.2 (CMe₃), 31.1 (CMe₃), 29.9 (CMe₃), 29.8 (CMe₃), 25.8 (CMe₃). HRMS (M/Z): calculated *M* = 519.3900; found 519.3959.

[(^{Me}NHO^{2ArO})Bi(μ -I)]₂ (3₂**)**

A 10 mL screw-cap vial fitted with a stir bar was charged with **L'H₃I** (0.100 g, 0.155 mmol) and suspended in 2 mL of toluene. Another 2 mL of a toluene solution of Bi(N(SiMe₃)₂)₃ (0.107 g, 0.155 mmol) was then added dropwise into the suspension. The reaction mixture was then stirred for 48 h to produce an orange suspension. The orange solid isolated by filtration was then washed with fresh toluene (3 \times 5 mL) and dried under vacuum to afford **3₂** (0.100 g, 0.117 mmol, 76%). X-ray quality single crystals were grown from a concentrated solution of a toluene/THF mixture at -30 °C.

¹H NMR (THF-D₈/C₆D₆ (2 : 5), 500 MHz): δ 7.48 (s, 1 H, ArH), 7.43 (s, 1 H, ArH), 6.76 (s, 1 H, ArH), 6.36 (s, 1 H, ArH), 6.34 (s, 1 H, NCHCHN), 6.03 (s, 1 H, NCHCHN), 5.79 (d, ²J_{HH} = 14 Hz, 1 H, ArCH₂N), 4.80 (s, 1 H, ArCHBi), 4.30 (d, ²J_{HH} = 14 Hz, 1 H, ArCH₂N), 3.33 (s, 3 H, NCH₃), 1.73 (s, 9 H, CMe₃), 1.62 (s, 9 H, CMe₃), 1.35 (s, 9 H, CMe₃), 1.32 (s, 9 H, CMe₃). ¹³C{¹H} NMR (THF-D₈/C₆D₆, (2 : 5) 126 MHz): 169.8 (NCN), 161.1 (Ar-C), 151.8 (Ar-C), 143.2 (Ar-C), 141.0 (Ar-C), 139.9 (Ar-C), 139.3 (Ar-C), 129.8 (Ar-C), 128.9 (Ar-C), 126.0 (Ar-C), 125.0 (Ar-C), 124.4 (Ar-C), 123.7 (Ar-C), 121.2 (NCHCHN), 120.3 (NCHCHN), 84.0 (CCHBi), 48.1 (ArCH₂N), 36.2 (N-Me), 35.9 (CMe₃), 35.7 (CMe₃), 34.5 (CMe₃), 34.4 (CMe₃), 32.6 (CMe₃), 32.5 (CMe₃), 31.7 (CMe₃), 30.4 (CMe₃). Elemental analysis of C₃₄H₄₈N₂O₂IBi: calculated C 47.89; H 5.67; N 3.29; found C 47.46; H 5.58; N 3.32.

[(^aL)BiBr₂(^{Dipp}Imd)] (4**)**

A 10 mL screw-cap vial fitted with a stir bar was charged with **LH₂Br** (0.528 g, 1.000 mmol) and suspended in 2 mL of toluene. Another 3 mL solution of Bi(N(SiMe₃)₂)₃ (0.345 g,

0.500 mmol) was added dropwise to the reaction vial. The reaction mixture was stirred for 48 h at room temperature to obtain an orange suspension. The orange solid isolated by filtration was washed with fresh toluene (3 \times 5 mL) and dried under vacuum to afford **4** (0.400 g, 0.384 mmol, 77%). X-ray quality single crystals were grown from concentrated solutions of a toluene/THF mixture at room temperature.

¹H NMR (CDCl₃, 500 MHz): δ 8.47 (s, 1 H, NCHN), 7.93 (s, 1 H, NCHN^{imd}), 7.61–7.15 (m, 10 H, ArH), 7.03 (s, 1 H, ArCH₂N), 6.86 (s, 1 H, ArCH₂N), 2.30 (br, m, 4 H, CHMe₂), 1.45 (s, 9 H, CMe₃), 1.25 (s, 9 H, CMe₃), 1.11 (d, ³J_{HH} = 7 Hz, 6 H, CHMe₂), 1.07 (d, ³J_{HH} = 7 Hz, 12 H, CHMe₂). ¹³C{¹H} NMR (CDCl₃, 126 MHz): 160.6 (NCCHN), 146.2 (NCHN), 145.6 (NCHN, Imd^{Dipp}), 141.9 (Ar-C), 140.0 (Ar-C), 139.8 (Ar-C), 138.2 (Ar-C), 137.9 (Ar-C), 133.5 (Ar-C), 132.4 (Ar-C), 131.6 (Ar-C), 130.7 (Ar-C), 130.1 (Ar-C), 129.2 (Ar-C), 125.1 (Ar-C), 124.7 (Ar-C), 124.5 (Ar-C), 123.8 (NCCHN), 123.1 (ACHCHN, Imd^{Dipp}), 121.6 (ACHCHN, Imd^{Dipp}), 53.3 (ArCH₂N), 35.4 (CHMe₂), 33.9 (CHMe₂), 31.9 (CMe₃), 31.2 (CMe₃), 28.6 (CMe₃), 28.2 (CMe₃), 24.4 (CHMe₂), 24.3 (CHMe₂), 24.2 (CHMe₂). Elemental Analysis of C₄₅H₆₁N₄OBr₂Bi: calculated C 51.83; H 5.90; N 5.37; found C 51.45; H 5.83; N 5.39.

Data availability

Synthetic descriptions of all reported compounds, spectroscopic data, computational details and coordinates, and crystallographic data files [CCDC 2348036 (**1**) 2348037 (**2**), 2348038 (**3₂**), 2348039 (**4**)†].

Conflicts of interest

There are no conflicts to declare.

Acknowledgements

D Mukherjee acknowledges SERB, India for SRG/2019/001931, CRG/2023/005396, and SB/S2/RJN-028/2018. D. Mallick thanks SERB, India for SRG/2019/001461 and additionally DST, India, for DST/NSM/R&D_HPC_Applications/2021/8 for providing computing resources of 'PARAM Shakti' at IIT Kharagpur and of 'PARAM Brahma' at IISER Pune. S. G. thanks CSIR-India, and S. S. thanks IISER Kolkata for their fellowships.

References

- (a) M. N. Hopkinson, C. Richter, M. Schedler and F. Glorius, *Nature*, 2014, **510**, 485–496; (b) D. Munz, *Organometallics*, 2018, **37**, 275–289; (c) V. Nesterov, D. Reiter, P. Bag, P. Frisch, R. Holzner, A. Porzelt and S. Inoue, *Chem. Rev.*, 2018, **118**, 9678–9842; (d) P. Bellotti, M. Koy, M. N. Hopkinson and F. Glorius, *Nat. Rev. Chem.*, 2021, **5**, 711–725.



- 2 (a) F. Pape and J. F. Teichert, *Eur. J. Org. Chem.*, 2017, **2017**, 4206–4229; (b) C. Fliedel, A. Labande, E. Manoury and R. Poli, *Coord. Chem. Rev.*, 2019, **394**, 65–103; (c) S. Hameury, P. de Frémont and P. Braunstein, *Chem. Soc. Rev.*, 2017, **46**, 632–733; (d) E. Peris and R. H. Crabtree, *Coord. Chem. Rev.*, 2004, **248**, 2239–2246.
- 3 Z. Li, P. Ji and J.-P. Cheng, *J. Org. Chem.*, 2021, **86**, 2974–2985.
- 4 (a) U. Gruseck and M. Heuschmann, *Chem. Ber.*, 2006, **120**, 2053–2064; (b) A. J. Arduengo III, R. L. Harlow and M. Kline, *J. Am. Chem. Soc.*, 1991, **113**, 361–363; (c) N. Kuhn, H. Bohnen, J. Kreutzberg, D. Bläser and R. Boese, *J. Chem. Soc., Chem. Commun.*, 1993, 1136–1137.
- 5 (a) M. G. D. Sharma, R. Dandela and V. Dhayalan, *Chem. – Eur. J.*, 2023, **29**, e202302106; (b) Q. Liang and D. Song, *Dalton Trans.*, 2022, **51**, 9191–9198; (c) S. Naumann, *Chem. Commun.*, 2019, **55**, 11658–11670; (d) A. Doddi, M. Peters and M. Tamm, *Chem. Rev.*, 2019, **119**, 6994–7112; (e) M. M. D. Roy and E. Rivard, *Acc. Chem. Res.*, 2017, **50**, 2017–2025; (f) R. S. Ghadwal, *Dalton Trans.*, 2016, **45**, 16081–16095; (g) R. D. Crocker and T. V. Nguyen, *Chem. – Eur. J.*, 2016, **22**, 2208–2213.
- 6 (a) M. Iglesias, A. Iturmendi, P. J. Sanz Miguel, V. Polo, J. J. Pérez-Torrente and L. A. Oro, *Chem. Commun.*, 2015, **51**, 12431–12434; (b) A. Iturmendi, N. García, E. A. Jaseer, J. Munárriz, P. J. Sanz Miguel, V. Polo, M. Iglesias and L. A. Oro, *Dalton Trans.*, 2016, **45**, 12835–12845.
- 7 A. Iturmendi, M. Iglesias, J. Munárriz, V. Polo, V. Passarelli, J. J. Pérez-Torrente and L. A. Oro, *Green Chem.*, 2018, **20**, 4875–4879.
- 8 A. Schumann and C. Hering-Junghans, *Eur. J. Inorg. Chem.*, 2018, **2018**, 2584–2588.
- 9 G. Song, X. Li, Z. Song, J. Zhao and H. Zhang, *Chem. – Eur. J.*, 2009, **15**, 5535–5544.
- 10 A. Petronilho, J. A. Woods, H. Mueller-Bunz, S. Bernhard and M. Albrecht, *Chem. – Eur. J.*, 2014, **20**, 15775–15784.
- 11 M. Kaur, K. Patra, N. U. D. Reshi and J. K. Bera, *Organometallics*, 2020, **39**, 189–200.
- 12 (a) N. R. Paisley, M. W. Lui, R. McDonald, M. J. Ferguson and E. Rivard, *Dalton Trans.*, 2016, **45**, 9860–9870; (b) M. W. Lui, O. Shynkaruk, M. S. Oakley, R. Sinelnikov, R. McDonald, M. J. Ferguson, A. Meldrum, M. Klobukowski and E. Rivard, *Dalton Trans.*, 2017, **46**, 5946–5954.
- 13 M. Viciano, M. Feliz, R. Corberán, J. A. Mata, E. Clot and E. Peris, *Organometallics*, 2007, **26**, 5304–5314.
- 14 (a) C. C. Chong, B. Rao, R. Ganguly, Y. Li and R. Kinjo, *Inorg. Chem.*, 2017, **56**, 8608–8614; (b) R. Guthardt, J. Mellin, C. Bruhn and U. Siemeling, *Eur. J. Inorg. Chem.*, 2021, **2022**, e202100903.
- 15 S. Wang, J. Yang, H. Zeng, Y. Zhou, F. Wang, X. Feng and S. Dong, *Org. Lett.*, 2023, **25**, 7247–7251.
- 16 (a) S. Goswami, P. Mandal, D. Mallick and D. Mukherjee, *Organometallics*, 2023, **42**, 1232–1241; (b) S. Goswami, P. Mandal, S. Sarkar, M. Mukherjee, S. Pal, D. Mallick and D. Mukherjee, *Dalton Trans.*, 2024, **53**, 1346–1354.
- 17 S. Goswami, S. Sarkar, D. Mallick and D. Mukherjee, *Organometallics*, 2024, **43**, 1308–1316.
- 18 (a) F. Wang, O. Planas and J. Cornella, *J. Am. Chem. Soc.*, 2019, **141**, 4235–4240; (b) O. Planas, F. Wang, M. Leutzsch and J. Cornella, *Science*, 2020, **367**, 313–317; (c) J. Cornella and Y. Pang, in *Comprehensive Organometallic Chemistry IV*, ed. G. Parkin, K. Meyer and D. O'hare, Elsevier, Oxford, 2022, pp. 478–522; (d) Y. Pang, N. Nothling, M. Leutzsch, L. Kang, E. Bill, M. van Gastel, E. Reijerse, R. Goddard, L. Wagner, D. SantaLucia, S. DeBeer, F. Neese and J. Cornella, *Science*, 2023, **380**, 1043–1048; (e) A. Stoy, M. Jurgensen, C. Millidoni, C. Berthold, J. Ramler, S. Martinez, M. R. Buchner and C. Lichtenberg, *Angew. Chem., Int. Ed.*, 2023, **62**, e202308293; (f) M. Mato and J. Cornella, *Angew. Chem., Int. Ed.*, 2024, **63**, e202315046.
- 19 (a) J. B. Waters, Q. Chen, T. A. Everitt and J. M. Goicoechea, *Dalton Trans.*, 2017, **46**, 12053–12066; (b) G. Wang, L. A. Freeman, D. A. Dickie, R. Mokrai, Z. Benkő and R. J. Gilliard, *Inorg. Chem.*, 2018, **57**, 11687–11695; (c) G. Wang, L. A. Freeman, D. A. Dickie, R. Mokrai, Z. Benkő and R. J. Gilliard Jr., *Chem. – Eur. J.*, 2019, **25**, 4335–4339; (d) L. P. Ho and M. Tamm, *Dalton Trans.*, 2021, **50**, 1202–1205; (e) M. M. Siddiqui, S. K. Sarkar, M. Nazish, M. Morganti, C. Köhler, J. Cai, L. Zhao, R. Herbst-Irmer, D. Stalke, G. Frenking and H. W. Roesky, *J. Am. Chem. Soc.*, 2021, **143**, 1301–1306; (f) J. E. Walley, L. S. Warring, G. Wang, D. A. Dickie, S. Pan, G. Frenking and R. J. Gilliard Jr., *Angew. Chem., Int. Ed.*, 2021, **60**, 6682–6690; (g) R. Deka and A. Orthaber, *Dalton Trans.*, 2022, **51**, 8540–8556.
- 20 <https://www.crystalimpact.com/diamond/>.
- 21 H. Aihara, T. Matsuo and H. Kawaguchi, *Chem. Commun.*, 2003, 2204–2205.
- 22 H. Steffenfauseweh, Y. V. Vishnevskiy, B. Neumann, H. G. Stammer, D. M. Andrada and R. S. Ghadwal, *Angew. Chem., Int. Ed.*, 2022, **61**, e202207415.
- 23 (a) R. H. Crabtree, *Coord. Chem. Rev.*, 2013, **257**, 755–766; (b) Á. Vivancos, C. Segarra and M. Albrecht, *Chem. Rev.*, 2018, **118**, 9493–9586; (c) S. C. Sau, P. K. Hota, S. K. Mandal, M. Soleilhavoup and G. Bertrand, *Chem. Soc. Rev.*, 2020, **49**, 1233–1252; (d) R. S. Ghadwal, *Angew. Chem., Int. Ed.*, 2023, **62**, e202304665.
- 24 C. Romain, C. Fliedel, S. Bellemin-Laponnaz and S. Dagorne, *Organometallics*, 2014, **33**, 5730–5739.
- 25 V. Dardun, L. Escomel, E. Jeanneau and C. Camp, *Dalton Trans.*, 2018, **47**, 10429–10433.
- 26 B. M. Day, T. Pugh, D. Hendriks, C. F. Guerra, D. J. Evans, F. M. Bickelhaupt and R. A. Layfield, *J. Am. Chem. Soc.*, 2013, **135**, 13338–13341.
- 27 (a) M. Uzelac, A. Hernán-Gómez, D. R. Armstrong, A. R. Kennedy and E. Hevia, *Chem. Sci.*, 2015, **6**, 5719–5728; (b) M. Wagner, T. Zöller, W. Hiller, M. H. Prosenc and K. Jurkschat, *Chem. Commun.*, 2013, **49**, 8925–8927.
- 28 M. Vehkamäki, T. Hatanpää, M. Ritala and M. Leskelä, *J. Mater. Chem.*, 2004, **14**, 3191–3197.
- 29 D. Zhang, H. Aihara, T. Watanabe, T. Matsuo and H. Kawaguchi, *J. Organomet. Chem.*, 2007, **692**, 234–242.

